^{8}Be and α decay of ^{16}O

M. Freer, N.M. Clarke, N. Curtis, B.R. Fulton, S.J. Hall, M.J. Leddy, J.S. Pople, G. Tungate, and R.P. Ward
School of Physics and Space Research, University of Birmingham, Birmingham, B15 2TT, United Kingdom

P.M. Simmons and W.D.M. Rae
Department of Physics, Nuclear Physics Laboratory, University of Oxford, Keble Road, Oxford, OX1 3RH, United Kingdom

S.P.G. Chappell, S.P. Fox, C.D. Jones, and D.L. Watson
Department of Physics, University of York, York, YO1 5DD, United Kingdom

G.J. Gyapong, S.M. Singer, and W.N. Catford
Department of Physics, University of Surrey, Guildford, Surrey, GU2 5XH, United Kingdom

P.H. Regan
Research School of Physical Sciences and Engineering, Australian National University, Canberra, Australia
(Received 13 October 1994)

The ^{12}C(^{16}O,4α)^{12}C reaction has been studied at a beam energy of 99 MeV. The data indicate the existence of sequential decays in the form $^{16}O^{*} \rightarrow 4\alpha$ in the exit channel. The excitation energy of the ^{16}O nucleus and the nature of the partition process leading to the 4α final state, has been reconstructed from the kinematics of the α particles. States have been observed at excitation energies of 17.1, 17.5, 18.0, 18.7, 19.3, and 21.4 MeV which decay into ^{8}Be+^{8}Be, ^{12}C(7.65 MeV, 0_2^+)+α and ^{12}C(9.64 MeV, 3^-)+α. Relative partial decay widths for these three channels have been measured. Angular correlation measurements have been used to deduce the spins of several of the observed states, and indicate spins in the range 2 to 6$\hbar$.

PACS number(s): 25.70.Ef, 25.70.Mn, 27.20.+n

I. INTRODUCTION

Considerable experimental and theoretical effort has been devoted to the understanding of the properties of the nucleus ^{16}O. From the experimental point of view, approximately 100 levels were discovered in ^{16}O below 20 MeV [1], over 50 of which were identified in a single study of resonances in the ^{12}C+α interaction [2]. Theoretically, ^{16}O has been extensively studied within the framework of many models, e.g., Hartree-Fock [3], shell model [4], alpha cluster model [5], cranked Nilsson-Strutinsky formalism [6], cluster-core model [7] and others. These models quite successfully describe the behavior of the low lying levels in ^{16}O up to excitation energies of about 12 MeV.

However, the interpretation of the majority of the levels between 10 and 20 MeV is significantly more complicated. Many of the models predict rotational behavior based on various ^{16}O configurations, but direct comparison with the experimentally established levels remains limited, since it is unclear which of the experimental states are linked by a common rotational structure. In fact, only one positive parity rotational band has been confidently assigned in this nucleus: the K=0 band, built on the 6.05 MeV first excited state, which is established up to 6^+ (16.28 MeV), and possibly 8^+ (22.5 MeV [8] or 29 MeV [9,10]). This rotational structure is believed to possess a 4p-4h configuration.

Many of the models [5,6] predict a rotational sequence based on an 8p-8h configuration. The moment of inertia of this structure is large, and would correspond to a ^{16}O configuration consisting of a linear chain of four alpha particles. Since the ^{8}Be nucleus is believed to possess a very deformed structure [11], resonances associated with such an ^{16}O configuration might be expected to couple strongly to the ^{8}Be decay channel. Possible candidates for this configuration have been reported in a study of the ^{12}C(α,^{8}Be)^{8}Be reaction [12]. In this instance selected resonances, up to a spin of 6^+, were demonstrated to lie on a $J(J+1)$ trajectory with $\hbar^2/2\mathcal{I}$=64 keV, consistent with a linear chain of four alpha particles. It should, however, be noted that in addition to the resonances which follow the rotational trend, there are resonances in the same data which do not. Furthermore, later studies of the ^{12}C(α,^{8}Be)^{8}Be reaction at higher energies failed to find any 8^+ candidate for such a band [13,14]. Consequently, the association of the ^{12}C(α,^{8}Be)^{8}Be resonances with the ^{16}O chain is not established unambiguously.

The present work involved a search for highly deformed structures in ^{16}O, excited in the interaction with a ^{12}C nucleus. The decay modes of particular interest were the breakup of the ^{16}O nuclei into ^{8}Be+^{8}Be and ^{12}C(7.65 MeV, 0_2^+)+α, since both of these final states involved deformed nuclei. Studies of the properties of the ^{12}C 7.65 MeV, 0_2^+ state [15] suggests that the nucleus is extremely deformed, which has prompted a link between this state and the 3α chain configuration.

II. RESULTS AND ANALYSIS

The ^{12}C(^{16}O,^{16}O*)^{12}C reaction was studied at the Australian National University 14UD tandem at a beam energy of 99 MeV, and with 100 μg cm^{-2} natural carbon target foils. The decay of the excited ^{16}O nucleus into a final state consisting of four alpha particles was detected in two adjacent 5×5 cm^2 position sensitive silicon strip detectors (PSSSD's) placed on one side of the beam axis. A single PSSSD was positioned on the other side of the beam axis to detect the recoiling ^{12}C nucleus. The PSSSD's each possessed 16 horizontal p-type strips on the front face, onto which a resistive layer had been implanted, which gave a resistively determined position response. The high degree of uniformity of this layer resulted in a position response which was linear to within a few percent. The position resolution was less than 200 μm [16]. The detectors were mounted 12.5 cm from the target at +24.5°, +52.5° and -30.5°. The two adjacent PSSSD's were coupled by connecting the adjacent strip ends together, such that the two detectors functioned as a single detector with, effectively, 16 10 cm horizontal strips.

This detection system allowed a study of the ^{12}C(^{16}O,4α)^{12}C reaction, in which the energy, angle, and detection time of all the exit channel particles could be recorded. The overdetermination of the reaction characteristics provided a means for the cross correlation of reaction parameters in order to obtain a data set with a low degree of background contamination. Figure 1 shows the Q-value spectrum for events in which four particles were detected in the coupled PSSSD's and one in the single PSSSD. The exit channel state of interest can be clearly identified with the peak at a Q value of −14.43 MeV. The peak at −18.87 MeV corresponds to the ^{12}C in its first excited state.

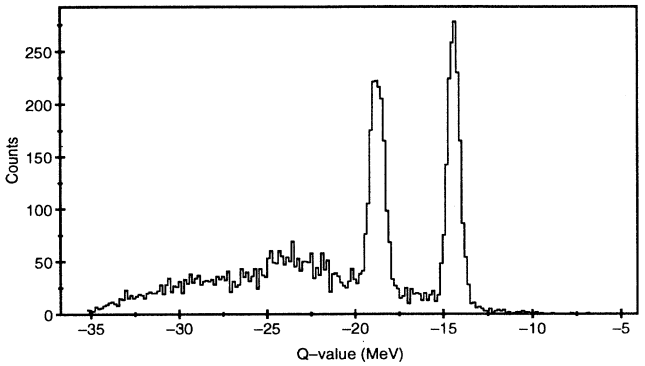

FIG. 1. Q-value spectrum for the ^{12}C(^{16}O,4α)^{12}C reaction. The two peaks correspond to the ^{12}C recoil being detected in the ground and first excited states.

For events for which it is established that the four alpha particles come from the decay of an excited ^{16}O, the excitation energy can be reconstructed from the momenta of the four alpha particles, through the relationship

$$E_x(^{16}\mathrm{O}) = E_{\mathrm{thresh}} + \sum_{i=1}^{4} E_i(\alpha) - E(^{16}\mathrm{O}) \ , \qquad (1)$$

where

$$E(^{16}\mathrm{O}) = \frac{\left[\left(\sum_{i=1}^{4} P_{\alpha_i}(x)\right)^2 + \left(\sum_{i=1}^{4} P_{\alpha_i}(y)\right)^2 + \left(\sum_{i=1}^{4} P_{\alpha_i}(z)\right)^2\right]}{2M(^{16}\mathrm{O})} . \qquad (2)$$

Here, E_{thresh} is the ^{16}O→4α breakup threshold energy (14.433 MeV) and $P_{\alpha_i}(x)$, $P_{\alpha_i}(y)$, and $P_{\alpha_i}(z)$ are the x, y, and z momentum components of the alpha particles. Equations (1) and (2), importantly, produce an ^{16}O excitation energy spectrum which is independent of the details of the successive emission of the four alpha particles. The ^{16}O excitation energy spectrum can also be calculated from the kinematics of the fifth detected particle, assuming it to be a ^{12}C nucleus. However, the energy resolution for the detection of the ^{12}C recoil (~400 keV) provided a poorer determination of the ^{16}O excitation energy than from the reconstruction of the four alpha particles, where the energy is determined by the position response of the detection system. The ^{16}O excitation energy spectrum, resulting from the application of Eq. (1), is shown in Fig. 2, for all 4α events in which the ^{12}C recoil was in the ground state. A number of states appear to be observed in the energy interval 16 – 22 MeV. The experimental resolution for the reconstruction of the excitation energy of the ^{16}O nucleus was ~350 keV.

Through the detection of the four alpha particles, the

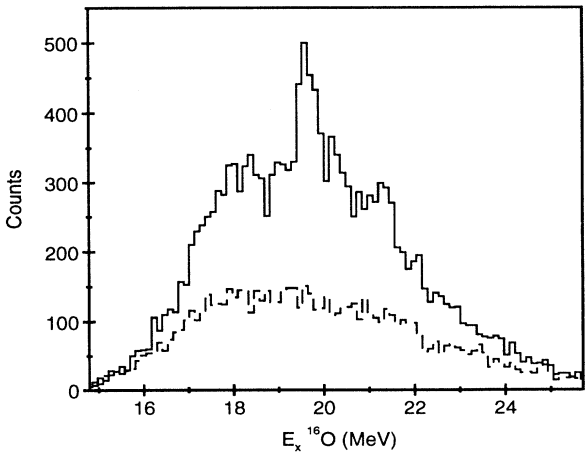

FIG. 2. ^{16}O excitation energy spectrum for decays leading to a 4α + ^{12}C$_{gs}$ final state. The dashed histogram is the estimated background.

process by which the ^{16}O excited state decayed may be reconstructed. The most important decay mechanisms which may be observed in this experiment are (i) the symmetric decay into two ^{8}Be nuclei, which then in turn decay into four alpha particles; (ii) α decay to the ^{12}C(7.65 MeV, 0_2^+) excited state, which then decays to ^{8}Be+α; and (iii) decay to the ^{12}C(9.64 MeV, 3^-) excited state in ^{12}C, which also decays to ^{8}Be+α. It is also possible for the states in ^{16}O to decay to other excited states in ^{12}C or ^{8}Be, for example the 10.3 MeV state in ^{12}C. However, the decay to this state cannot be differentiated from the background owing to the large width of this state ($\Gamma \sim 3$ MeV). Similarly, decays to the first excited state in ^{8}Be cannot be readily resolved from the background in this measurement. The details of the decay were determined as described below, and Fig. 3 shows the ^{16}O excitation energy spectra produced by the three scenarios, and with the ^{12}C recoil in the ground [Figs. 3(a)–(c)] or first excited states [Figs. 3(d)–(f)].

In order to determine that, for example, two ^{8}Be nuclei were produced, the excitation energies in two ^{8}Be nuclei were constructed from all possible pairs of the four particles in turn. The ^{8}Be excitation energies for all combinations have been incremented into the spectrum shown Fig. 4(a). Each pair was then checked to determine whether it fell within the peak at 92 keV above the ^{8}Be$\rightarrow 2\alpha$ decay threshold. The possible combinations of the alpha particles were (1-2, 3-4 : 1-3, 2-4 : 1-4, 2-3). In a similar fashion, the four alpha particles were tested in groups of three to determine if they originated from a ^{12}C nucleus with excitation energies of 7.65 or 9.64 MeV (1-2-3 : 1-2-4 : 1-3-4 : 2-3-4), see Fig. 4(b). The ^{16}O excitation energy spectra formed by these procedures are shown in Figs. 3(b) and 3(c). Clearly the nature of this selection process leads to a background contamination of the various ^{16}O excitation energy spectra, due to the chance that the alpha particles coincidentally satisfy the various conditions for the decay channel selection. The level of background has been indicated on the various excitation energy spectra in Fig. 3. This was generated by placing condition gates adjacent to excitation energy peaks in the ^{8}Be and ^{12}C spectra in each instance.

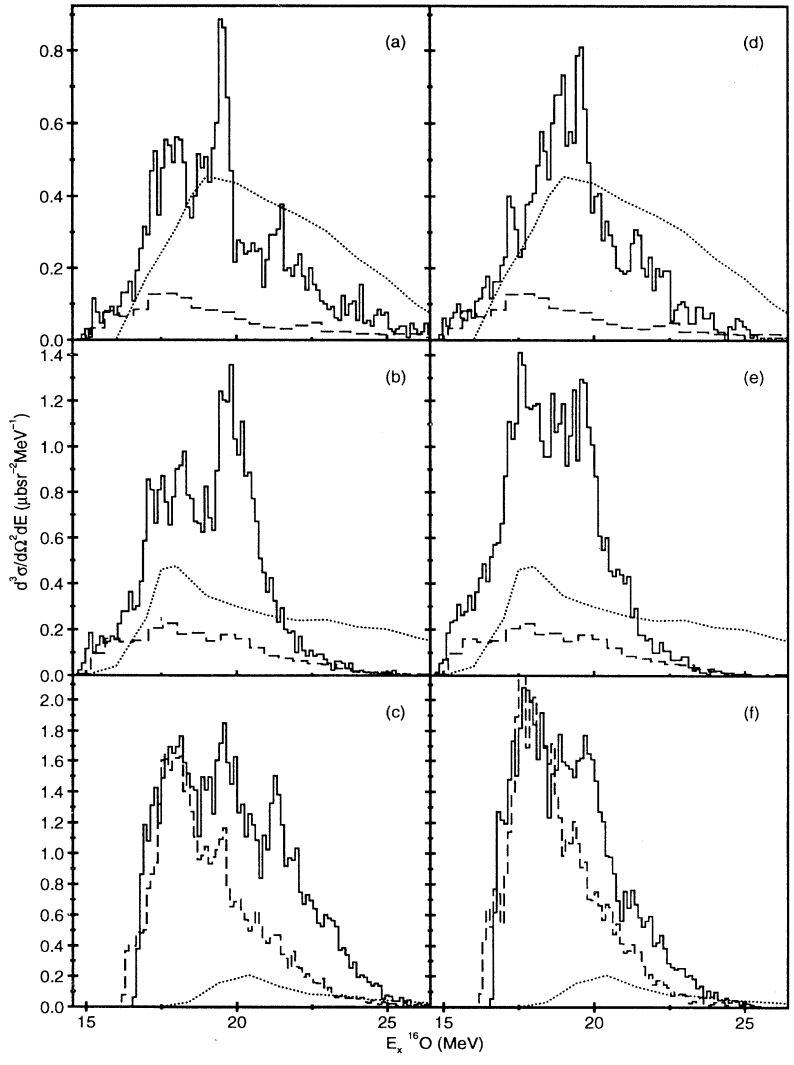

FIG. 3. ^{16}O excitation energy spectra for the various decay channels.
(a) ^{12}C[^{16}O,^{8} Be +^{8} Be]^{12}C$_{gs}$,
(b) ^{12}C[^{16}O,^{12} C(0_2^+) + α]^{12}C$_{gs}$,
(c) ^{12}C[^{16}O,^{12} C(3^-) + α]^{12}C$_{gs}$,
(d) ^{12}C(^{16}O,^{8} Be +^{8} Be)^{12}C(2^+),
(e) ^{12}C[^{16}O,^{12} C(0_2^+) + α]^{12}C(2^+) and
(f) ^{12}C[^{16}O,^{12} C(3^-) + α] ^{12}C(2^+). The dashed histograms are estimates of the background contributions to each of the spectra. The dotted lines are the Monte Carlo efficiency calculations which include the effects of the Coulomb barrier. The detection efficiencies are plotted such that the vertical scale reads twice the detection efficiency measured in percent.

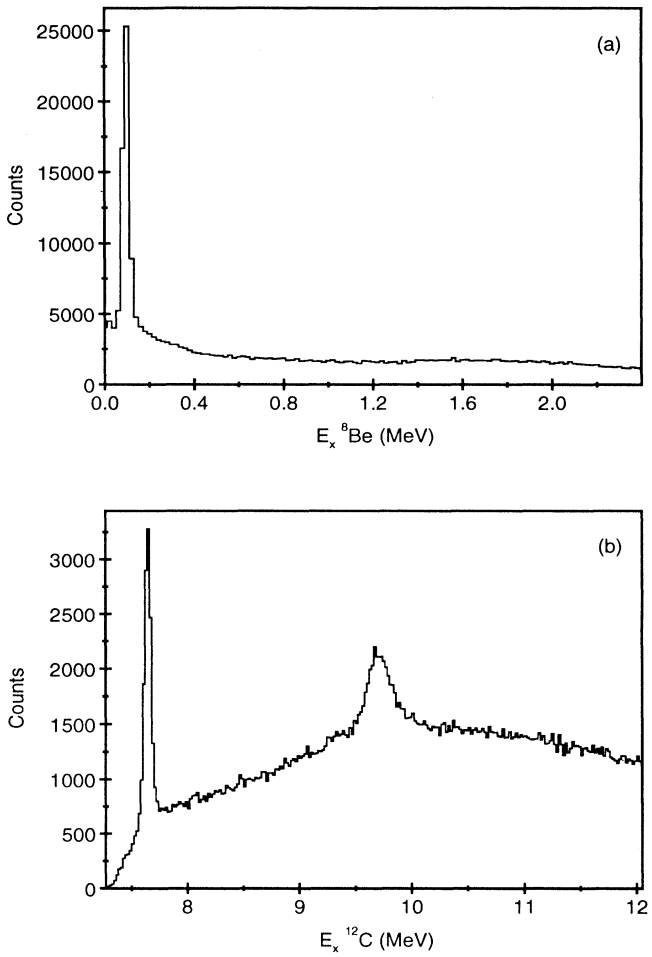

FIG. 4. (a) ^{8}Be excitation energy spectrum calculated for all alpha pairs. (b) ^{12}C excitation energy spectrum calculated for all possible combinations of three alpha particles (see the text for details).

The background can originate from several sources; (i) random coincidences between reaction products from different beam, target interactions, or (ii) reactions in which the four alpha particles were not produced from the decay of a ^{16}O nucleus. Examples of reactions which could produce such contributions are ^{12}C(^{16}O,^{12}Cα)^{12}C(0_2^+) and ^{12}C(^{16}O,^{12}C^{8}Be)^{8}Be. Figures 5(a) and 5(b) show the spectra in Figs. 3(b) and 3(a) [$E_x(^{16}\mathrm{O})_1$] plotted against the calculated excitation energies in ^{16}O [$E_x(^{16}\mathrm{O})_2$] and ^{20}Ne, respectively. Figure 5(a) has been produced by gating on events in which three alpha particles came from the decay of the ^{12}C, 0_2^+ state, and Fig. 5(b) corresponds to events in which the four alpha particles were produced from the decay of two $^{8}\mathrm{Be}_{gs}$ nuclei. There appears to be no evidence for contributions to these spectra from discrete states in either ^{20}Ne or ^{16}O, decaying into ^{8}Be $+^{12}\mathrm{C}_{gs}$ and $^{12}\mathrm{C}_{gs} + \alpha$, respectively, which would appear as vertical loci. Figure 5(a) does indicate an increased intensity in the region $E_x(^{16}\mathrm{O})_2$ >25 MeV. However, the appearance of common peaks in projected $E_x(^{16}\mathrm{O})_1$ spectra, produced under the conditions $E_x(^{16}\mathrm{O})_2$ >25 MeV and $E_x(^{16}\mathrm{O})_2$ <25 MeV, suggests that this structure is related to the ^{12}C(0_2^+)+α decay channel. Similar analysis of other spectra in Figs. 2 and 3 also indicates that the above reactions are not present in these data.

The results of Monte Carlo calculations of the efficiency with which the detection system can detect the products from the various reactions are also shown in Fig. 3. These profiles include the effect of the Coulomb barrier for each channel, which determines the low excitation energy limit of the data. The Monte Carlo code generated particles assuming a primary angular distribution which was isotropic in the center of mass, and for the subsequent decay sequence of the excited ^{16}O nucleus, isotropic or $1/\sin\theta$ angular distributions were used for decay of zero spin and nonzero spin states, respectively. The multiple particle detection process was then simulated in detail, including energy thresholds of the detector signals and the rejection of events in which two

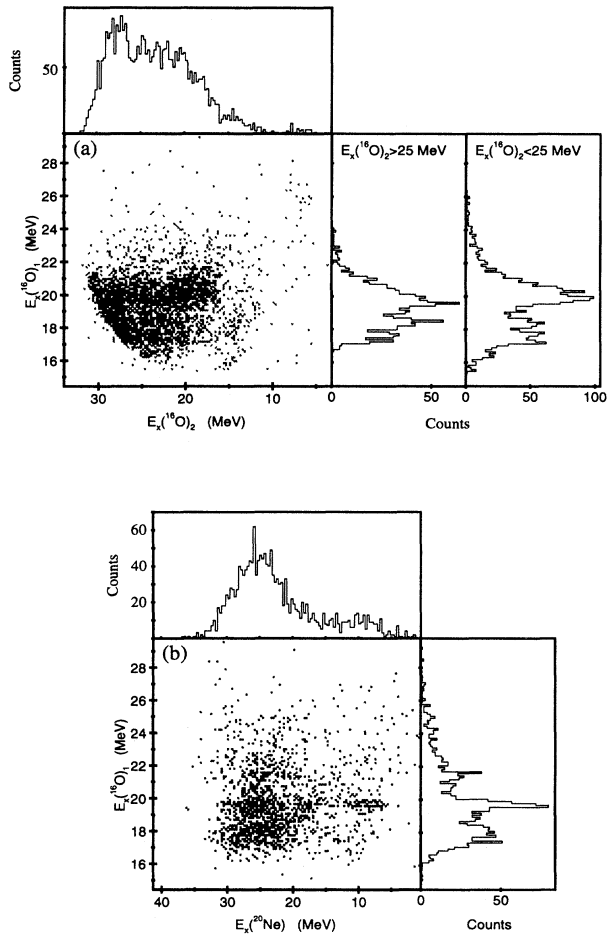

FIG. 5. The ^{16}O excitation energy spectra from Figs. 3(b) and 3(a) [$E_x(^{16}\mathrm{O})_1$] plotted against the calculated excitation energy in (a) ^{16}O [$E_x(^{16}\mathrm{O})_2$] and (b) ^{20}Ne, corresponding to the reactions ^{12}C(^{16}O,^{12}Cα)^{12}C(0_2^+) and ^{12}C(^{16}O,^{12}C^{8}Be)^{8}Be, respectively. The data in (a) have been projected onto the $E_x(^{16}\mathrm{O})_1$ axis under the different conditions that $E_x(^{16}\mathrm{O})_2$ <25 MeV and $E_x(^{16}\mathrm{O})_2$ >25 MeV.

particles entered the same strip.

The various decay paths produce nuclei with differing binding energies and spin. Consequently, the energy and angular distributions of the alpha particles differ widely, which is reflected in the efficiency profiles. These Monte Carlo and Coulomb barrier profiles are not intended to reproduce the details of the spectra, since additional factors such as the decay phase space and structural properties of the states modify the intensity of the data. However, the calculations can be used to extract the relative strengths for the states to decay into the various channels.

The three spectra which correspond to an excited ^{16}O nucleus in coincidence with a ^{12}C recoil in the ground state possess several common features. Figure 3(a) indicates that there are states at energies of 17.11, 17.5, 18.0, 18.7, 19.3, and 21.4 MeV, which decay into two ^{8}Be nuclei. The first five of these states can also be seen in the ^{12}C(0_2^+) decay channel. In contrast with the ^{8}Be+^{8}Be decay channel, odd spin states may be observed in the ^{12}C(0_2^+)+α decay branch. This may account for the differences between the spectra in Figs. 3(a) and 3(b). For instance the high energy shoulder which appears on the side of the state at 19.3 MeV in the ^{12}C(0_2^+)+α spectrum may be associated with an odd spin state. Furthermore, the 21.4 MeV state in this alpha decay channel might be obscured by the additional yield which lies in this region. Interestingly, the states at 19.3 and 21.4 MeV are observed strongly in the ^{12}C(3^-)-α decay channel, which might indicate that the state at 21.4 MeV has high spin and for this reason the decay to the ^{12}C(0_2^+) state is inhibited.

For comparison, the excitation energy spectra in Figs. 3(d) – 3(f), which correspond to the ^{12}C recoil in the 4.43 MeV, 2^+ state, are shown. Since the angular momenta involved in these reactions differ from when the recoil is in the ground state, the associated ^{16}O spectra are generally different. However, there appears to be substantial evidence for the states identified above, and in particular the state at 19.3 MeV is consistently reproduced.

A. Angular Correlations

The angular correlations between the final state nuclei can reveal many features of the reaction process. The gross nature of the correlations may be used to determine the spins of the nuclei, in many cases in a model independent manner, whilst the fine detail may in conjunction with reaction models reveal the m-substate populations [17]. The center of mass angles which have been used to describe the correlations follow from the scheme of Rae and Bhowmik [18]. The angle θ^* describes the scattering process in the primary center of mass system, and ψ defines the emission angle of the decay products with respect to the beam axis in the second center of mass frame. In this measurement, angular correlations have been studied for states in ^{16}O which decay into the partitions ^{8}Be+^{8}Be and ^{12}C(0_2^+)+α, since both these final states consist of spin-zero nuclei. In the instance that all initial and final state particles are spin zero, the angular correlations are considerably simplified. At the scattering angle $\theta^*=0°$, where only the $m=0$ substate is populated in the excited ^{16}O nucleus, and hence the correlations follow the form,

$$W(\psi) = |P_J(\cos\psi)|^2 , \tag{3}$$

where J is the spin of the excited ^{16}O nucleus. Thus, if the correlations span this scattering angle region, a model independent spin determination may be achieved.

Da Silviera [19] demonstrated that at nonzero scattering angles the phase of the correlation structure shifts such that

$$\Delta\psi = \Delta\theta^* \frac{l_{gf}}{J}, \tag{4}$$

hence the periodicity of the correlation structure resembles

$$W(\psi) = |P_J[\cos(\psi_0 + \Delta\psi)]|^2 , \tag{5}$$

where l_{gf} and J are the final state grazing angular momentum and the spin of the excited ^{16}O nucleus, respectively, and ψ_0 is the value of ψ evaluated at $\theta^*=0°$.

This classical prescription is founded on the assumption that the primary reaction proceeds through a narrow angular momentum window, i.e., only a few values of l_{gi} and l_{gf} contribute to the cross section, and the ^{16}O nucleus decays through particle emission in a direction perpendicular to the angular momentum axis (**J**). Under these conditions there is a direct relationship between **J** and $\mathbf{l}_{gf}$ (i.e., $\mathbf{l}_{gf}= \mathbf{l}_{gi}$-**J**), and thus l_{gf}/J is uniquely defined. This classical result was validated by Marsh and Rae [20] with a quantum mechanical description of the reaction process. Since $\Delta\psi$ varies linearly with respect to θ^*, then the resulting correlation pattern takes on the form of ridges with a gradient l_{gf}/J, which provides a method for determining l_{gf} and also further verifying J.

However, both the classical and quantum mechanical descriptions of the correlation structure are only valid for relatively small scattering angles ($\theta^* < 30°$), and the ^{12}C(^{16}O,^{8}Be^{8}Be)^{12}C and ^{12}C[^{16}O,^{12}C(0_2^+)α]^{12}C reaction data span a region around $\theta^* = 90°$.

The angular correlations, examples of which are shown in Fig. 6, indicate that the correlation structure is still present at large scattering angles. They have been analyzed by projecting the data onto the $\theta^*=90°$, ψ axis at an angle which is parallel to the observed ridge structure. This procedure statistically enhances the relative intensities of the maxima and minima in the correlation pattern.

In order to extract the angular momenta producing the correlation patterns, the projected data have been compared to correlations calculated using a single partial wave model. In the instance that the reaction proceeds through a single entrance channel partial wave, the transition amplitudes may be written in the form [17]

$$T_J^m(\theta^*) = \sum_{m_i}\sum_{m_f} \langle l_{gi} m_i l_{gf} m_f J m\rangle \times Y_{l_{gi}}^{m_i}(0,0) Y_{l_{gf}}^{m_f}(\theta^*,0), \tag{6}$$

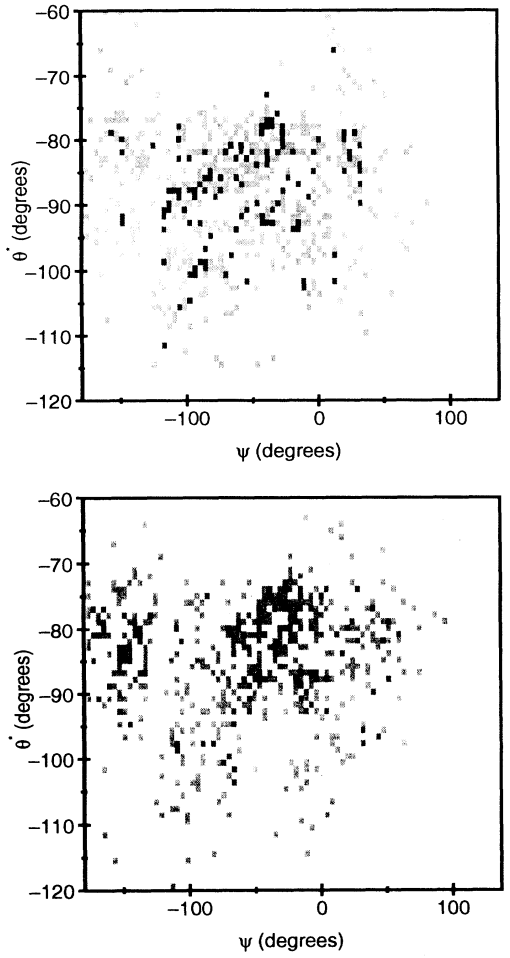

FIG. 6. Angular correlation plots for the decay of the states at (a) 18.0 MeV and (b) 19.3 MeV, into the $^{12}C(0_2^+)+\alpha$ channel.

where we consider only the scattering in the reaction plane ($\phi = 0$). This restriction is effectively imposed in the experiment by the reduced detection efficiency for the out-of-plane reactions. Thus, the double differential cross section is

$$\frac{d^2\sigma}{d\Omega^2} = \left| \sum_m T_J^m(\theta^*) Y_J^m(\psi, 0) \right|^2 . \quad (7)$$

In this analysis the dominant entrance channel partial wave was deduced from an analysis of the angular distributions for the reaction $^{12}C[^{16}O,^{12}C(0_2^+)]^{16}O$, at the beam energy of 99 MeV. The scattering angle distribution was highly oscillatory with a period characteristic of $l_{gi}=18\pm1\hbar$. These data were acquired simultaneously with the main data stream by employing a lower multiplicity trigger condition on the data stream selection. The exit channel partial waves may take values between $l_{gi} - J$ and $l_{gi} + J$. The choice of the exit channel partial wave distribution determines the nature of the correlation structure, and in particular the gradient of the ridges. In this analysis $l_{gf}=l_{gi} - J$ was used to generate the correlations, this value reproduces the behavior of the angular correlations in a number of other reactions [17,21], and is in agreement with the classical model of Da Silviera.

The correlations predicted by this simple model were modified according to the acceptance cuts of the detection system. The in-plane reaction kinematics were calculated for each θ^*, ψ angular combination, and the resulting energies and angles of the particles were tested against the experimental acceptances. The calculated acceptances reproduced the general features of the data, although detailed agreement was not achieved since in order to make the calculations simple, the reaction was treated as a three-body final state, i.e., ^{8}Be+^{8}Be+^{12}C or $^{12}C(0_2^+)+\alpha+^{12}C$, and the out-of-plane behavior of the experimental data was neglected in these calculations. The resulting correlations were then projected in the same manner as the data.

It should be stressed that this correlation analysis is not aimed at providing a full fit to the data. Rather, it provides a means whereby the main features of the correlations can be calculated, with the explicit inclusion of the experimental acceptances.

The quality of the correlation structures is sufficient that spins may be inferred for several of the states observed. The angular correlation projections, from which the spins have been inferred, are shown in Fig. 7. Since the projections were made so as to enhance the correlation structure, and then projected onto the ψ=90° axis, the peaks in the spectra do not quite align with the maxima in an associated $P_J(\cos\psi)$. However, the calculated correlations, with which the data are compared, also contain these slight distortions.

The combined correlation projections for the two states at 17.1 and 17.5 MeV are shown in Figs. 7(a) and 7(b) for the decay into ^{8}Be+^{8}Be and $^{12}C(0_2^+)+\alpha$, respectively. Both of the projections demonstrate good agreement with the dependence calculated for $J = 2$. Figures 7(c) and 7(f) show the projections for the 19.3 MeV state corresponding to the symmetric and asymmetric decay respectively. These data indicate a J=4 dependence. The projected correlation in Fig. 7(f) indicates that there is some contribution from the shoulder on this peak which is observed in Fig. 3(b), since the quality of the periodic structure appears diminished. The correlation projection for the state at 21.4 MeV appearing in the ^{8}Be+^{8}Be decay channel [Fig. 7(e)] is restricted due to the limited experimental acceptance. Nevertheless, the structure around 0° supports the suggested spin of J=6. A J=8 calculation is also shown, this appears to reproduce the periodicity but not the phase of the experimental yield. However, for this particular state the phase of the projected J=8 correlation is sensitive to the value of l_{gi}. Consequently, wider angular coverage is required in order to make a more definite statement of the spin of this state.

The correlation for the state at 18.0 MeV [Fig. 7(d)] is more complicated. The positions of the maxima and minima have a periodicity which is similar to a J=2 Legendre polynomial, but occurs 45° out of phase with those in Figs. 7(a) and 7(b). Since the state appears in the symmetric decay channel, this indicates that the state

has even spin. Hence, it is likely that this peak corresponds to a coherent superposition of even spin states, perhaps $J=2$ and $J=4$ as shown in the figure. Furthermore, the lack of a distinct minimum in the correlation would also seem to confirm this interpretation. However, due to the limited angular coverage, it is not possible to draw firmer conclusions as to the nature of this peak. All other features in the excitation spectra were analyzed, but no clear correlation structure was observed.

Figures 7(g) to 7(l) show the experimental projected

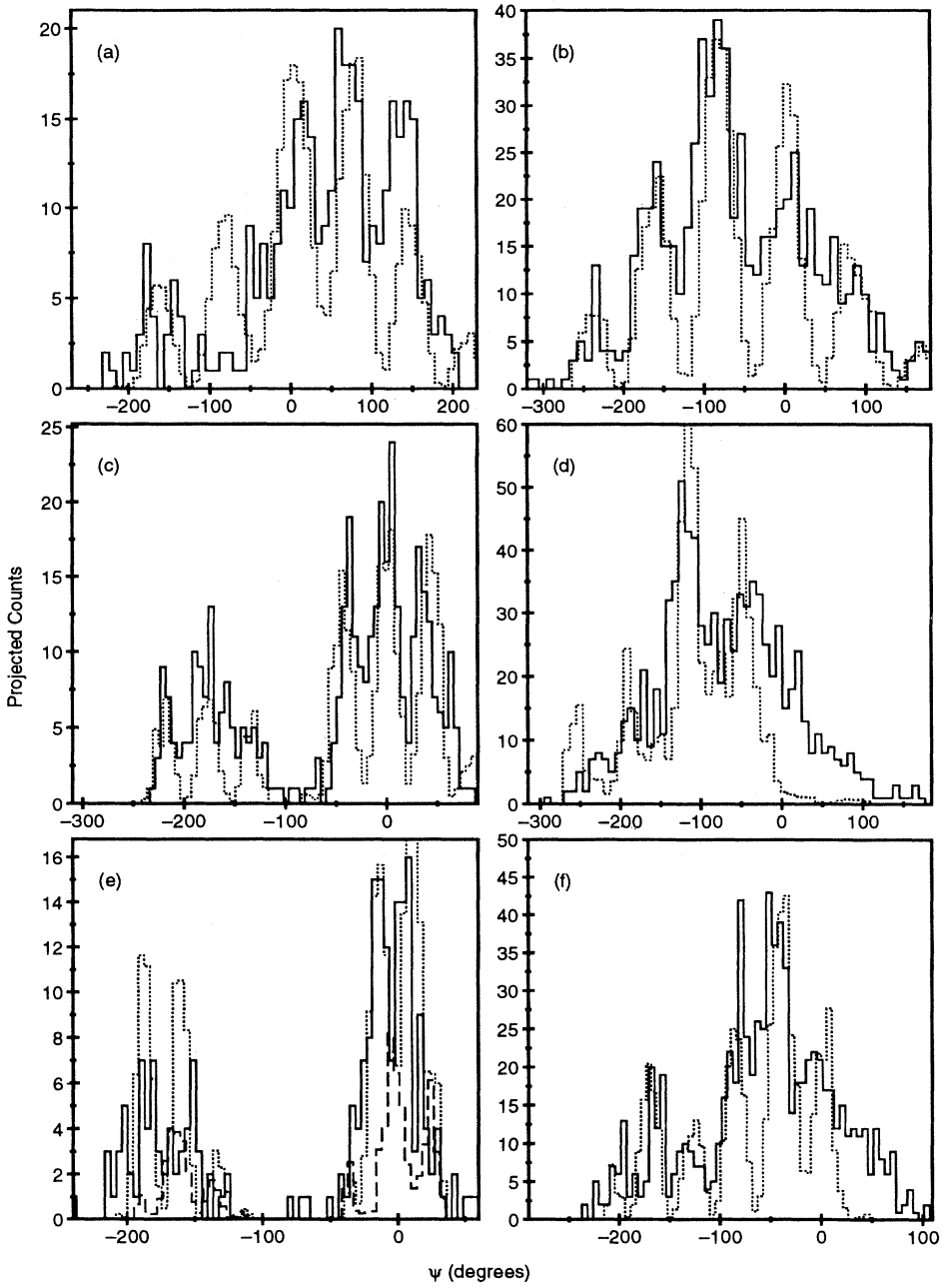

FIG. 7. The experimental angular correlation projections (solid histograms) and the projected calculated correlations (dotted histograms), for the (a) 17.1 and 17.5 MeV states, decaying into the ^{8}Be+^{8}Be channel with a $J=2$ calculation; (b) 17.1 and 17.5 MeV states, decaying into the ^{12}C(0_2^+)+α channel with a $J=2$ calculation; (c) 19.3 MeV state, decaying into the ^{8}Be+^{8}Be channel with a $J=4$ calculation; (d) 18.0 MeV state, decaying into the ^{12}C(0_2^+)+α channel with a $J=4$+$J=2$ calculated correlation; (e) 21.4 MeV state, decaying into the ^{8}Be+^{8}Be channel with a $J=6$ (dotted histogram) and $J=8$ (dashed histogram) calculations; (f) 19.3 MeV state, decaying into the ^{12}C(0_2^+)+α channel with a $J=4$ calculation; (g) as (a) but with a $J=4$ calculated distribution; (h) as (b) but with a $J=4$ calculated distribution; (i) and (j) as (c) but with a $J=2$ and a $J=6$ calculated distribution, respectively; and (k) and (l) as (f) but with a $J=2$ and a $J=6$ calculated distribution, respectively.

TABLE I. Gradients of the experimental angular correlations and the deduced entrance channel grazing angular momentum.

E_x(MeV)	$J(\hbar)$	$\Delta\theta^*/\Delta\psi$	l_{gi} $(\hbar)$
17.1 and 17.5	2	0.119 ± 0.01[a]	18.8 ± 1.3
		0.126 ± 0.01[b]	17.8 ± 1.3
18.0	(2,4)	0.131 ± 0.01[b]	
19.3	4	0.284 ± 0.02[a]	18.1 ± 1.3
		0.269 ± 0.02[b]	18.8 ± 1.3
21.4	(6)	0.632 ± 0.06[a]	15.5 ± 2.4

[a]Deduced from the ^{8}Be+^{8}Be decay.
[b]Deduced from the ^{12}C$(0_2^+)+\alpha$ decay.

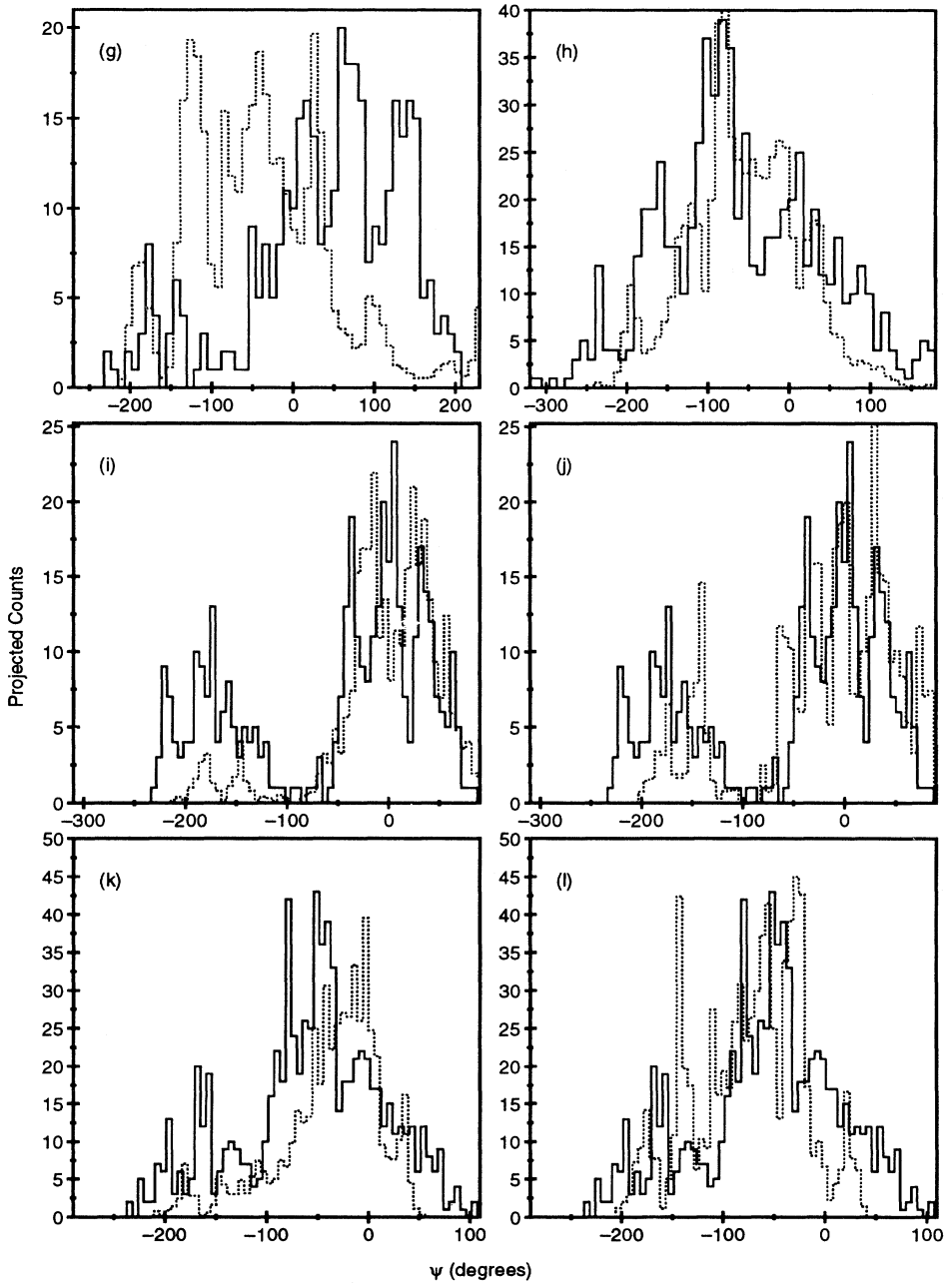

FIG. 7. (*Continued*).

TABLE II. Relative partial decay widths for the three decay channels observed in the experiment. The values calculated using the statistical model code STATIS [24], are also shown.

E_x (MeV)	$J(\hbar)$	$\Gamma_{^8Be}/\Gamma_{^{12}C(0_2^+)}$		$\Gamma_{^8Be}/\Gamma_{^{12}C(3^-)}$		$\Gamma_{^{12}C(0_2^+)}/\Gamma_{^{12}C(3^-)}$	
		Expt.	Calc.	Expt.	Calc.	Expt.	Calc.
17.1	2	0.65±0.16	1.31±0.08	-	-	-	-
17.5	2	0.72±0.18	1.33±0.08	-	-	-	-
19.3	4	0.47±0.15	1.15±0.02	0.24±0.08	0.031±0.020	0.51±0.15	0.031±0.015
21.4	6	>3±1.10	1.16±0.03	0.16±0.06	0.043±0.019	<0.05±0.02	0.037±0.018

angular correlations, for the states at 17.1, 17.5, and 19.3 MeV, compared with calculations for alternative spins. These calculations have been projected at the same angle as the experimental data. Consequently, the degree of structure in these latter figures is considerably reduced, as is the quality of the agreement with the experimental data. For example, the J=4 calculation in Fig. 7(g), neither reproduces the general structure nor the periodicity of the data. One exception is Fig. 7(j), which shows that the J=6 calculation can reproduce some of the structure of the experimental data for the 19.3 MeV state decaying into the ^{8}Be +^{8} Be channel. This is due to the relatively restricted angular coverage for this state in this particular decay channel. However, the J=6 calculation cannot reproduce the correlation structure for the same state but in the $^{12}C(0_2^+)$-α decay channel [Fig. 7(l)], for which there is wider angular coverage.

Both the data and calculations confirm the existence of a ridge structure in the correlations around the θ^*=90° angular region, as was also observed by Rae [22,23]. In fact the calculations indicate that the ridge structure persists over the entire range of scattering angles ($0° \leq \theta^* \leq 180°$), and the gradient is consistent with the classically determined value ($\Delta\theta^*/\Delta\psi = J/l_{gf}$), if l_{gf} is constrained such that $l_{gf}=l_{gi}-J$. This value of the final state angular momentum has been shown to reproduce the behavior of the angular correlations for other reaction systems [17,21]. Hence, this would suggest that the gradients of the correlation patterns may be used to indicate the angular momenta involved the the reaction process. Table I lists the gradients at which the projections used to produce the plots in Fig. 7 were performed. Equation (4) has been used to deduce the entrance channel grazing angular momentum for those states for which we have been able to infer spins. The projection gradients and the inferred spins are consistent with a grazing angular momentum of ~18$\hbar$. This result confirms the predictions of the calculated correlations, namely, that the gradient of the correlation pattern remains nearly constant. This further indicates that the reaction mechanism involved in the excitation process is limited to a few partial waves around the grazing angular momentum.

The consistency between the various approaches to the analysis further strengthens the proposed spins.

B. Partial decay widths

The relative partial decay widths $\Gamma_{^8Be}/\Gamma_{^{12}C(0_2^+)}$, $\Gamma_{^8Be}/\Gamma_{^{12}C(3^-)}$, and $\Gamma_{^{12}C(0_2^+)}/\Gamma_{^{12}C(3^-)}$ are shown in Table II for each of the states for which spin have been inferred. These have been calculated by normalizing the yield in each channel to the detection efficiency, such that

$$\frac{\Gamma_{^8Be}}{\Gamma_{^{12}C(0_2^+)}} = \frac{\text{Yield}(^8\text{Be})}{\text{Yield}[^{12}\text{C}(0_2^+)]} \frac{\text{Efficiency}[^{12}\text{C}(0_2^+)]}{\text{Efficiency}(^8\text{Be})}. \quad (8)$$

These relative partial decay widths have been compared with statistical model calculations performed with the code STATIS [24]. The optical model parameters used for these calculations are taken from Brochard *et al.* [13], where a study of the reaction yields in the ^{12}C+α interaction was made with the Hauser-Feshbach formalism. The reader is referred to [13] for a more detailed description of the parameters used in these calculations. The potentials for the two decay channels of interest are reproduced in Table III. The ^{8}Be+^{8}Be potential used by these authors is particularly shallow; this was required in order to reproduce the experimental cross sections. The sensitivity of the calculated partial decay widths to the choice of optical model parameters would suggest that the uncertainty in the individual decay widths is of the order of 20-50 %. However these uncertainties cancel to some extent in the calculated ratios of the decay widths, resulting in the errors shown in Table II. Similarly, the systematic uncertainties in the Monte Carlo calculations, which only approximate the angular distributions for the scattering and decay processes, are estimated to give a ~30% error in the relative efficiencies. These errors are spin dependent and have been estimated from a comparison of the 1/sinψ angular distribution, used in the Monte Carlo calculations, and Legendre polynomials, over the

TABLE III. Optical model parameters for the two decay channels of interest. See reference [13] for more details.

Channel	U (MeV)	r_U (fm)	a_U (fm)	W (MeV)	r_W (fm)	a_W (fm)
^{12}C+α	185.0	1.4	0.52	25.0	1.4	0.52
^{8}Be+^{8}Be	10.6	1.4	0.45	0.1	1.4	0.45

angular region of the experimental correlations. These errors reflect the influence on the calculated efficiency of the different ψ angular coverage in the various decay channels. The uncertainty in the θ^* angular dependence of the Monte Carlo calculations is less important as the angular correlations for all the decay channels span the same θ^* region for a given ^{16}O excitation energy.

A comparison of the experimental and statistical model values indicates that for the 19.3 MeV state the $^{12}C(0_2^+)$ and ^{8}Be decay branches are favoured over the α decay to the $^{12}C(3^-)$ state in excess of statistical expectations by at least one order of magnitude. The 21.4 MeV state again has an enhanced probability for the decay into ^{8}Be+^{8}Be. However, the relative yields for the α decay to the two states in ^{12}C appear to be in closer agreement with statistical expectations. The overall preference of the decay of these states into the ^{8}Be+^{8}Be and $^{12}C(0_2^+)+\alpha$ channels suggests that the states observed have a much closer structural link with these final states than with a ^{12}C nucleus in the 3^- state. Since these preferred decay channels contain highly deformed nuclei, this indicates that the ^{16}O states may also be associated with a very deformed configuration.

However, it must be noted that the calculations suggest that there should be an equivalent suppression of the 21.4 MeV state in both the ^{8}Be+^{8}Be and $^{12}C(0_2^+)+\alpha$ decay channels, when compared to the $^{12}C(3^-)$ α decay channel. This feature is not observed, which may indicate that this state exhibits a preference for the ^{8}Be+^{8}Be decay channel, or alternatively points to the unsuitability of the potentials used in these calculations.

III. DISCUSSION AND CONCLUSIONS

A comparison of the states found in this work with those contained in the literature reveals some similarities. For example, a number of the resonances observed by Ames [2] in $^{12}C+\alpha$ scattering data may be associated with those observed in this work. Nevertheless, given the sheer number of resonances observed, this correspondence could be coincidental. In addition, the states at 17.1, 17.5, and 18.0 MeV may be associated with the resonances observed in the $^{12}C(\alpha,^8Be)^8Be$ data of Chevallier [12] and Brochard [13]. Curiously, however, there is no agreement with the 19.3 MeV, 4^+ state, which coincides with a 6^+ resonance [12], and the state at 21.4 MeV, (6^+) has no counterpart in either sets of data. The lack of correlation between the higher excitation energy portion ($E_x > 18$ MeV) of these data, and the resonances observed in the $^{12}C(\alpha,^8Be)^8Be$ reaction, may indicate that two different reaction mechanisms are populating different structures.

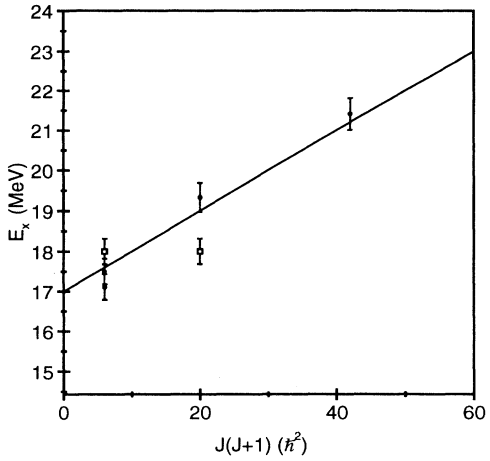

FIG. 8. Energy-spin systematics of the states for which spins were inferred. The open squares show the 18.0 MeV state with both $J=2$ and $J=4$.

The energy-spin systematics of the present data are shown in Fig. 8. These appear to lie on a rotational, $J(J+1)$, trajectory, with $\hbar^2/2\mathcal{I}=95\pm20$ keV and a bandhead energy of 17.0 ± 0.7 MeV. If indeed these states are candidates for a new rotational structure, then the associated moment of inertia would suggest a nuclear configuration which is extremely deformed. Furthermore, the preferential decay of these states into channels comprised of deformed nuclei also points to the degree of deformation of the states in ^{16}O.

ACKNOWLEDGMENTS

M.F., N.C., M.J.L., J.S.P., S.M.S., S.P.G.C., S.P.F., and P.M.S. would like to thank the Engineering and Physical Sciences Research Council for financial support.

[1] F. Ajzenberg-Selove, Nucl. Phys. **A460**, 1 (1986).
[2] L.L. Ames, Phys. Rev. C **25**, 729 (1982).
[3] J.P. Svenne, in *Advances in Nuclear Physics*, edited by J.W. Negele and E. Vogt (Plenum, New York, 1979), Vol. 11, p. 179.
[4] J.M. Irvine, C.D. Latorre, and V.F.E. Pucknell, Adv. Phys. **20**, 661 (1971).
[5] W. Bauhoff, H. Schultheis, and R. Schultheis, Phys. Rev. C **29**, 1046 (1984).
[6] S. Aberg, I. Ragnarsson, T. Bengtsson, and R. Sheline, Nucl. Phys. **A391**, 327 (1982).
[7] B. Buck, C.B. Dover, and J.P. Vary, Phys. Rev. C **11**, 1803 (1975).
[8] S.J. Sanders, L.M. Martz, and P.D. Parker, Phys. Rev. C **20**, 1743 (1979).
[9] W.D.M. Rae, S.C. Allcock, S. Marsh, and B.R. Fulton, Phys. Lett. **156B**, 167 (1985).
[10] W.D.M. Rae, S.C. Allcock, and J. Zhang, Nucl. Phys. **A568**, 287 (1994).
[11] A.B. Volkov, Nucl. Phys. **74**, 33 (1965).

[12] P. Chevallier, F. Scheibling, G. Goldring, I. Plesser, and M.W. Sachs, Phys. Rev. **160**, 827 (1967).
[13] F. Brochard, P. Chevallier, D. Disdier, V. Rauch, G. Rudolf, and F. Scheibling, Phys. Rev. C **13**, 967 (1976).
[14] Ph. Martin and T.R. Ophel, Nucl. Phys. **A194**, 491 (1972).
[15] N. Takigawa and A. Arima, Nucl. Phys. **A168**, 593 (1971).
[16] N. Curtis *et al.*, Nucl. Instrum. Methods A **351**, 359 (1994).
[17] F. Pougheon, P. Roussel, M. Bernas, F. Diaf, B. Fabbro, F. Naulin, E. Plagnol, and G. Rotbard, Nucl. Phys. **A325**, 481 (1979).
[18] W.D.M. Rae and R.K. Bhowmik, Nucl. Phys. **A420**, 320 (1984).
[19] E.F. Da Silviera, in Proceedings of the 14th Winter Meeting on Nuclear Physics, Bormio, 1976 (unpublished).
[20] S. Marsh and D.M. Rae, Phys. Lett. **153B**, 21 (1985).
[21] B.R. Fulton, S.J. Bennett, M. Freer, J.T. Murgatroyd, G.J. Gyapong, N.S. Jarvis, C.D. Jones, D.L. Watson, J.D. Brown, W.D.M. Rae, A.E. Smith, and J.S. Lilley, Phys. Lett. B **267**, 325 (1991).
[22] W.D.M. Rae, P.R. Keeling, and S.C. Allcock, Phys. Lett. B **184**, 133(1987).
[23] W.D.M. Rae, P.R. Keeling, and A.E. Smith, Phys. Lett. B **198**, 49 (1987).
[24] R.G. Stokstad, Hauser-Feshbach code STATIS, Yale University, Wright Nuclear Structure Laboratory Report 52, 1972 (unpublished).